Solid-State Synthesis, Crystal Structure, and Effective Third-Order Nonlinear Optical Properties of $(NEt_4)_3[MoOS_3Cu_3Br_3(\mu_2\text{-}Br)]\cdot 2H_2O$

Shu Shi*

Optical Crystal Laboratory and Department of Chemical Engineering, National University of Singapore, Singapore

Zhangrong Chen, Hongwei Hou, and Xinquan Xin

Department of Chemistry, Nanjing University, Nanjing, China

Kaibei Yu

Chengdu Center of Analysis and Determination, Academia Sinica, Chengdu, China

Received January 24, 1995. Revised Manuscript Received June 8, 1995[⊗]

The title compound $[NEt_4]_3[MoOS_3Cu_3Br_3(\mu_2\text{-}Br)]\cdot 2H_2O$ was synthesized by a solid-state reaction of $(NH_4)_2MoO_2S_2$, CuBr, and Et_4NBr at 70 °C. Single-crystal X-ray diffraction data show that the anionic cluster $[MoOS_3(CuBr)_3(\mu\text{-}Br)]^{3-}$ has a half-open-cage structure which is an intermediate between cubic cage and nest structures. The crystal has an orthorhombic symmetry with a space group of *Pnma*. Cell parameters are $a = 18.648(3)$ Å, $b = 15.156(2)$ Å, $c = 16.226(3)$ Å, $V = 4586$ Å^3, and $Z = 4$. The crystal structure was refined to $R = 0.061$, $R_w = 0.053$. The cluster exhibits both optical self-defocusing and optical nonlinear absorption (effectively $n_2 = -2.3 \times 10^{-16}$ m^2 W^{-1}, $\alpha_2 = 1.6 \times 10^{-10}$ m W^{-1} in a 1.9×10^{-3} mol dm^{-3} acetonitrile solution) as measured with a 7-ns pulsed laser at 532 nm. The corresponding effective third-order nonlinear optical susceptibilities ($\chi^{(3)}$) is 5.4×10^{-10} esu. These nonlinear optical properties of the cluster were compared with those of cubic-cage-shaped and nest-shaped clusters to reveal a qualitative structure/NLO property correlation.

Introduction

Metal chalcogenide clusters have been studied extensively in the past because of their relevance to biological systems and in catalytic processes.[1-8] Yet until recently, no one has noticed that they also exhibit very interesting nonlinear optical (NLO) properties.[9,10] Experimental results obtained in acetonitrile solution with 7-ns pulsed laser at 532 nm show that some Cu–Mo(W)–S clusters exhibit very strong NLO effects. Among the clusters studied are cubic-cage-shaped $(n\text{-}Bu_4N)_3[MS_4M'_3BrX_3]$ (M = Mo, W; M′ = Cu, Ag; X = Cl, Br, I),[9,10] nest-shaped $(n\text{-}Bu_4N)_2[MoOS_3Cu_3X'_3]$ (X′ = NCS, Cl, and Br), twin-nest-shaped $(n\text{-}Et_4N)_4[Mo_2O_2S_6Cu_6Br_2I_4]$,[11-14] and butterfly-shaped $MOS_3Cu_2(PPh_3)_x$ (M = Mo, W; x = 3, 4).[15] It was discovered that all of the cubic-cage-shaped Cu(Ag)–Mo(W)–S clusters, $(n\text{-}Bu_4N)_3[MS_4M'_3BrX_3]$, exhibit strong nonlinear absorption and negligibly small nonlinear refraction (self-focusing), while both the nest-shaped clusters $(n\text{-}Bu_4N)_2[MoOS_3Cu_3X'_3]$ and the twin-nest-shaped cluster $(n\text{-}Et_4N)_4]Mo_2O_2S_6Cu_6Br_2I_4]$ exhibit a strong self-defocusing effect. Structurally, the nest-shaped MoS_3Cu_3 skeleton of the $(n\text{-}Bu_4N)_2[MoOS_3Cu_3X'_3]$ cluster can be considered as a derivative (with one vertex, Br, missing) of the cubic-cage-shaped MoS_3Cu_3Br core of the $(n\text{-}Bu_4N)_3[MoS_4Cu_3BrX_3]$ clusters. In this paper we report the synthesis, characterization, and NLO properties of a new cluster, $(NEt_4)_3[MoOS_3Cu_3Br_3(\mu_2\text{-}Br)]\cdot 2H_2O$, which assumes an intermediate structure between the cubic cage and nest structures.

Experimental Section

Materials. Compound $(NH_4)MoO_2S_2$ was prepared according to literature.[16] Other chemicals were purchased as A.R. grade reagents and used without further purification.

Synthesis of $(NEt_4)_3[MoOS_3Cu_3Br_3(\mu_2\text{-}Br)]\cdot 2H_2O$. A reaction tube containing a well-ground mixture of $(NH_4)_2MoO_2S_2$ (0.23 g, 1 mmol), CuBr (0.29 g, 2 mmol), and Et_4NBr (0.42 g,

* To whom correspondence should be addressed.

[⊗] Abstract published in *Advance ACS Abstracts,* July 15, 1995.

(1) Mueller, A.; Dartmann, M.; Romer, C.; Clegg, W.; Sheldrick, G. M. *Angew. Chem., Int. Ed. Engl.* **1981**, *20*, 1060.
(2) Mueller, A.; Dremann, E.; Joster, R.; Bogge, H. *Angew. Chem., Int. Ed. Engl.* **1981**, *20*, 934.
(3) Sarkar, S.; Mishra, S. B. S. *Coord. Chem. Rev.* **1984**, *59*, 239.
(4) Holm, R. H. *Chem. Soc. Rev.* **1981**, *10*, 455.
(5) Jeannin, Y.; Secheresse, F.; Bernes, S.; Robert, F. *Inorg. Chim. Acta* **1992**, *198*, 493.
(6) Lang, J. P.; Xin, X. Q. *J. Solid State Chem.* **1994**, *108*, 118.
(7) Gheller, S. F.; Hambley, T. W.; Rodgess, J. R.; Brownlee, R. T. C.; O'connor, M. J.; Snow, M. R.; Wedd, A. G. *Inorg. Chem.* **1984**, *23*, 2519.
(8) Simhon, E. D.; Baenziger, N. C.; Kanatzidis, M.; Draganjac, M.; Couconvanis, D. *J. Am. Chem. Soc.* **1981**, *103*, 1218.
(9) Shi, S.; Ji, W.; Tang, S. H.; Lang, J. P.; Xin, X. Q. *J. Am. Chem. Soc.* **1994**, *116*, 3615.
(10) Shi, S,; Ji, W.; Lang, J. P.; Xin, X. Q. *J. Phys. Chem.* **1994**, *98*, 3570.
(11) Hou, H. W.; Xin, X. Q.; Liu, J. Chen, M. Q.; Shi, S. *J. Chem. Soc., Dalton Trans.* **1994**, 3211.
(12) Shi, S.; Ji, W.; Xie, W.; Chong, T. C.; Zeng, H. C.; Lang, J. P.; Xin, X. Q. *Mater. Chem. Phys.* **1995**, *39*, 298.
(13) Hou, H. W.; Ye, X. R., Liu, J.; Chen, M. Q.; Shi, S. *Chem. Mater.* **1995**, *7*, 472.
(14) Shi, S.; Wei, J.; Xin, X. Q. *J. Phys. Chem.* **1995**, *99*, 894.
(15) Shi, S.; Hou, H. W.; Xin, X. Q. *J. Phys. Chem.* **1995**, *99*, 4050.
(16) McDonald, J. W.; Frieson, G. D.; Rosenhein, L. D.; Newton, W. E. *Inorg. Chim. Acta* **1983**, *72*, 205.

0897-4756/95/2807-1519$09.00/0

2 mmol) was heated at 70 °C for 12 h under pure nitrogen. Extraction of the resultant dark red solid with CH_2Cl_2 (20 mL) and filtration afforded a deep red clean solution. Black hexagonal crystals were obtained from the extract after a large portion of the solvent was slowly evaporated; yield 0.14 g. Anal. (Calcd) for $C_{24}H_{64}N_3Br_4Cu_3MoO_3S_3$: C, 25.12 (25.16); H, 5.27 (5.59); N, 3.23 (3.23); Cu, 19.62 (19.60); Mo, 8.37 (8.07). IR spectra (KBr pellets): ν(Mo−O_{term}), 911 cm^{-1}; ν(Mo−S_{br}), 445 cm^{-1}.

Crystal Structure Analysis. The X-ray diffraction data of a crystal of $(NEt_4)_3[MoOS_3Cu_3Br_3(\mu_2\text{-}Br)]\cdot 2H_2O$ were collected with an R3M/E four-circle X-ray diffractometer (Mo Kα radiation, λ = 0.710 73 Å) equipped with a graphite monochromator.

The diffraction data were treated sequentially by an intensity decay correction, an empirical absorption correction and the Lorentz correction. The crystal parameters of the compound are listed in Table 1. The structure of $(NEt_4)_3[MoOS_3Cu_3Br_3(\mu_2\text{-}Br)]\cdot 2H_2O$ was solved by direct methods. Hydrogen atoms were included in the refinement but restrained to ride on the atom to which they are bonded except for the hydrogen atoms bonded to C(10), C(12), $O_w(1)$, and $O_w(2)$. Final atomic coordinates and isotropic thermal parameters of the cluster are given in Table 2.

Other Characterizations. Carbon, hydrogen, and nitrogen analyses were performed on a PE 240C elemental analyzer. Copper and molybdenum were analyzed with a JA 1100 + 2000 ICP quantometer. Infrared spectra were recorded on a Fourier Nicolet FT-10SX spectrometer with pressed KBr pellets. Electronic spectra were taken on a Shimadzu UV-240. Cyclic voltammogram was determined with a PN 270 electrochemical analyzer, using platinum as a working electrode. The measurement was conducted in a CH_3CN solution under nitrogen atmosphere with 0.1 mol dm^{-3} Et_4NClO_4 as supporting electrolyte.

Nonlinear Optical Measurements. The nonlinear optical responses of the compound in CH_3CN solution (contained in a 1-mm-thick quartz cuvette) were investigated with linearly polarized optical pulses from a Q-switched frequency-doubled Nd:YAG laser. Pulse duration (full width of 1/*e* maximum in irradiance) was measured to be 7 ± 1 ns. Spatial profiles of the optical pulses were nearly Gaussian after passing through a spatial filter. Two types of experiments were conducted to measure the NLO properties.

(1) A Z-scan experiment[17] was conducted to determine relative importance of NLO refraction versus NLO absorption of the cluster. The laser pulse were divided by a splitter into two beams. One beam was taken to measure the change of the incident light whereas the other was focused on to the sample. The minimum spot radius of the focused beam was 30 ± 5 μm (half-width of $1/e^2$ maximum in irradiance). Two energy probes (Laser Precision RjP-735) were used to detect energy of the two laser beams simultaneously. The probes sent signals to an energy radiometer (Laser Precision Rj7620) where the signals were digitized and further transferred to a computer.

The sample was mounted on a translation stage controlled by the computer. The NLO properties of the sample were manifested by moving the samples along the axis of the incident beam (Z-direction) with respect to the focal point. An aperture of 0.5 mm radius was placed in front of a detector that was positioned behind the sample to assist the measurement of the self-defocusing effect of the sample. To test the reliability of the Z-scan apparatus, we measured the third-order nonlinear refractive index, n_2, of CS_2 and obtained a value of (1.0 ± 0.4) × 10^{-11} esu, which is in good agreement with the reported value of 1.2 × 10^{-11} esu at 532 nm.[18]

(2) Temporal profiles of both the incident and transmitted pulses were studied with the same laser system. This was done by recording both types of temporal profiles simultaneously employing two fast-response photodetectors (Electro-Optics Technology ET2010, response time <1 ns). The signals of the photodetectors were displayed on a Tektronix 7104 oscilloscope, digitized by a CCD camera system, store and processed by the computer.

Table 1. Crystal Parameters of $(NEt_4)_3[MoOS_3Cu_3Br_3(\mu_2\text{-}Br)]\cdot 2H_2O$

formula	$C_{24}H_{64}N_3MoCu_3S_3O_3Br_4$
formula weight	1144.64
crystal system	orthorhombic
space group	*Pnma*
a (Å)	18.648(3)
b (Å)	15.156(2)
c (Å)	16.226(3)
V (Å^3)	4586(1)
Z	4
D_c (g cm^{-3})	1.66
F(000)	2280
absorption coefficient (cm^{-1})	52.43
intensity variation	less than 2.6%
scan type and rate	$\theta/2\theta$, 6.5°/min
2θ limits (deg)	2−46
measured data	3721
unique data	3621
observable data	with $I \geq 5\sigma(I)$: 1598
no. of variables	217
R	0.0605
R_w	0.0532
S	1.142
$\Delta\varrho_{max}$ (e Å^{-3})	1.044
$\Delta\varrho_{min}$ (e Å^{-3})	−0.484

Results and Discussion

Synthesis and Structure. The synthetic conditions for $[MoOS_3Cu_3Br_3(\mu_2\text{-}Br)]^{3-}$ is similar to those for cubic-cage-shaped clusters $[MS_4M'_3BrX_3]^{3-}$ (M = Mo, W; M' = Cu, Ag; X = Cl, Br, I) and nest-shaped clusters $[MoOS_3Cu_3X'_3]^{2-}$ (X' = NCS, Cl, Br). The differences are illustrated in eqs 1−4. When MoS_4^{2-} is reacted with

$$MoS_4^{2-} + 3CuX \longrightarrow [MoS_4Cu_3X_3]^{2-} + [MoS_4Cu_3X_3]_n^{2n-} \quad (1)$$

$$[MoS_4Cu_3X_3]_n^{2n-} \xrightarrow[\sim 100\ °C]{Br^-} [MoS_4Cu_3X_3(\mu_3\text{-}Br)]^{3-} \quad \text{cubic cage} \quad (2)$$

$$MoOS_3^{2-} + 3CuX + Br^- \xrightarrow{\sim 100\ °C} [MoOS_3Cu_3X_3]^{2-} \quad \text{nest} \quad (3)$$

$$MoO_2S_2^{2-} + 3CuX + Br^- \xrightarrow{\sim 70\ °C} [MoOS_3Cu_3X_3(\mu_2\text{-}Br)]^{3-} \quad \text{half-open cage} \quad (4)$$

3 equiv of CuX (X = halides, pseudo-halides), two types of $MoS_4Cu_3Br_3^{2-}$ clusters are formed (eqs 1 and 2). The first type has a relatively flattened structure (structure **I**) with all of the four S atoms in the MoS_4 unit

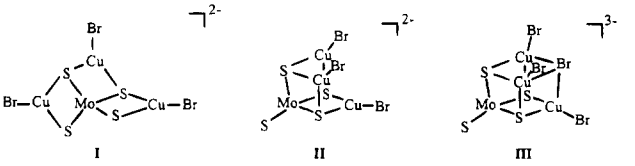

I II III

participating in coordination to Cu atoms. This type of clusters have a tendency to polymerize into two-dimensional sheets.[19,20] The second type has a nest-

(17) Sheik-Bahae, M.; Said, A. A.; Van Stryland, E. W. *Opt. Lett.* **1989**, *14*, 955.

(18) Sheik-Bahae, M.; Said, A. A.; Wei, T. H.; Hagan, D. J.; Van Stryland, E. W. *IEEE J. Quantum Electron* **1990**, *26*, 760.

(19) Manoli, J. M.; Potvin, C.; Secheresse, F.; Marzak, S. *Inorg. Chim. Acta* **1988**, *150*, 257.

Table 2. Atomic Coordinates ($\times 10^4$) and Isotropic Thermal Parameters (2×10^3) of $(NEt_4)_3[MoOS_3Cu_3Br_3(\mu_2\text{-}Br)]\cdot 2H_2O$

	X	Y	Z	U[a]
Mo	2918(1)	7500	2083(1)	69(1)
Br(1)	1557(1)	5128(1)	812(1)	99(1)
Br(2)	4801(1)	7500	−36(2)	129(1)
Br(3)	2346(1)	7500	−334(2)	94(1)
Cu(1)	3828(1)	7500	832(2)	91(1)
Cu(2)	2213(1)	6397(1)	1096(1)	88(1)
S(1)	3389(2)	6295(2)	1463(3)	81(1)
S(2)	1724(3)	7500	1864(4)	75(2)
N(1)	1505(8)	5055(12)	3723(7)	134(8)
N(2)	176(7)	2500	9923(14)	94(8)
O	3088(8)	7500	3108(9)	111(7)
Ow(1)	1104(13)	7500	6929(15)	481(46)
Ow(2)	2663(21)	2500	1750(20)	337(25)
C(1)	1381(12)	4088(14)	3732(12)	233(18)
C(2)	1169(23)	3676(24)	2920(24)	316(32)

[a] Equivalent isotropic U defined as one-third of the trace of the orthogonalized U_{ij} tensor.

shaped structure (structure **II**) with only three of the four S atoms from the MoS_4 unit involved in coordination to Cu atoms. This type of clusters can further react in the presence of Br^- to yield cage-shaped clusters (structure **III**). A series of cage-shaped clusters $[MS_4Cu_3BrX_3]^{3-}$ (M = Mo, W; X = Cl, Br, I) have been synthesized following this strategy.[9,10]

Formation of the polymeric product can be totally eliminated if the starting material, MoS_4^{2-} anion is replaced by $MoOS_3^{2-}$ (eq 3). This is because the terminal oxygen of the $MoOS_3$ unit has little tendency to coordinate to a copper atom. A series of nest-shaped clusters $[MoOS_3Cu_3X'_3]^{2-}$ have been synthesized[11-13] by taking advantage of the low reactivity ("directing effect") of this terminal oxygen.

With slightly different starting materials and reaction condition, the half-open-cage-shaped cluster, $[MoOS_3Cu_3Br_3(\mu_2\text{-}Br)]^{3-}$, was formed. The ORTEP of the anionic cluster of the title compound, $[MoOS_3Cu_3Br_3(\mu_2\text{-}Br)]^{3-}$, is shown in Figure 1. Packing of the compound in a unit cell is displayed in Figure 2. The skeleton of the anionic cluster consists of one Mo, three μ_3-S, three Cu, and one μ_2-Br atoms. The anion has a symmetry plane, passing through the O, Mo, S(2), Cu(1), Br(2), and Br(3) atoms.

The Mo atom has basically retained the tetrahedral geometry of the free $[MoOS_3]^{2-}$ anion. Three CuBr groups are bonded to the $[MoOS_3]^{2-}$ tetrahedron across three S···S edges. The fourth Br atom, Br(3), binds to only two of the three Cu atoms of the cluster, Cu(2) and Cu(2a). These two Cu atoms adopt a distorted tetrahedral geometry, coordinated with two Br and two S atoms. Atom Cu(1) is in a trigonal-planar environment, coordinated with one Br and two S atoms. Atom Br(3) is out of the plane containing Cu(2a), S(2), and Cu(2) atoms, further apart from Cu(1) atom. The Cu(1)−Br(3) distance (3.350 Å) is much longer than Cu(2)−Br(3) [or Cu(2a)−Br(3)] distance (2.870 Å). Selected bond lengths and bond angles are listed in Tables 3 and 4, respectively.

We noted that all the Cu atoms in the cage-shaped clusters adopt a pseudotetrahedron coordination environment, whereas all the Cu atoms in the nest-shaped clusters adopt pseudotrigonal-planar coordination environment. The half-open-cage structure of $[MoOS_3Cu_3Br_3(\mu_2\text{-}Br)]^{3-}$ placed itself in a unique position between those two extreme cases. Both the pseudotetrahedron and the pseudotrigonal-planar coordination modes of Cu are found in $[MoOS_3Cu_3Br_3(\mu_2\text{-}Br)]^{3-}$.

Electronic Spectrum and Cyclic Voltammogram. The electronic spectrum of $(NEt_4)_3[MoOS_3Cu_3Br_3(\mu_2\text{-}Br)]\cdot 2H_2O$ is shown in Figure 3. Absorption peaks were observed at the following wavelengths (extinction coefficients): 501.2 nm (1.65×10^3 cm^{-1} mol^{-1} dm^3); 408.4 nm (7.80×10^3 cm^{-1} mol^{-1} dm^3); 287.4 nm (1.21×10^4 cm^{-1} mol^{-1} dm^3). Because the S→Mo charge-transfer bands are significantly affected by the coordination of $MoOS_3^{2-}$ to Cu (through $Cu(S)_2Mo$ bonds), shifting of the electronic transition bands of $(NEt_4)_3[MoOS_3Cu_3Br_3(\mu_2\text{-}Br)]\cdot 2H_2O$ was observed in comparison to $MoOS_3^{2-}$ moiety. The optical absorption peak with longest wavelength in $MoOS_3^{2-}$ (459 nm) is shifted to longer wavelength in $[MoOS_3Cu_3Br_3(\mu_2\text{-}Br)]^{3-}$ (501.2 nm). The cyclic voltammogram of $[MoOS_3Cu_3Br_3(\mu_2\text{-}Br)]^{3-}$ contains two quasireversible redox couples (E_{pa1} = 0.40 V and E_{pc1} = 0.51 V; E_{pa2} = −1.75 V and E_{pc2} = −1.53 V). We believe that the E_{pa1} wave is related to Cu, whereas the E_{pa2} wave is related to the Mo atom.

NLO Effects and Its Electronic Origin. The cluster exhibits both NLO absorption and NLO refraction as will be described later. Since the cluster has a linear absorption peak at 501 nm, it is possible that absorption of laser light by the solution may result in a temperature gradient and consequently cause a refractive index change in the solution, $\Delta n = (dn/dT)\Delta T = n_2'I$. A dn/dT value of -4.5×10^{-4} K^{-1} is known for the solvent acetonitrile.[21] On the other hand, whether or not the thermal lensing effect ($\Delta n = (dn/dT)\Delta T$) can be observed within a time window of a few nanoseconds depends on detailed focus geometry of the measurement apparatus. The rise time needed for a thermal lensing effect to come into play after the arrival of a laser pulse is dictated by the acoustic transit time, ω_0/v_s, where ω_0 is the waist of the laser beam and v_s the sound velocity in the solvent.

We have demonstrated in our earlier publications that the rise time (a delay time needed for the thermal effect to manifest itself) is much longer than 10 ns in acetonitrile solutions under a focus geometry nearly identical with that used in this experiment and that the thermal effect is unlikely to be responsible for the NLO effect observed within the first few nanoseconds after the arrival of a laser pulse.[12,14]

To confirm this point, we compared the widths (fwhm) of the temporal profiles of the transmitted laser pulses with those of the incident pulses obtained over an incident peak irradiance range of 20−200 MW cm^{-2}. The observed width of the temporal profiles of the transmitted laser pulses are slightly wider than those of the incident pulses. If the refractive index change of the sample is caused by a local temperature rise due to the absorption of light energy (an accumulative process), it will take at least a few microseconds (after the laser pulse hits the sample) for the refractive index to resume its original value. Consequently, the tempo-

(20) Secheresse, F.; Bernes, S.; Robert, F.; Jeannin, Y. *J. Chem. Soc., Dalton Trans.* **1991**, 2875.

(21) Riddick, J. A.; Bunger, W. B.; Sakano, T. K. *Organic Solvents: Physical Properties and Method of Purification*, 4th ed.; John Wiley & Sons: New York, 1986.

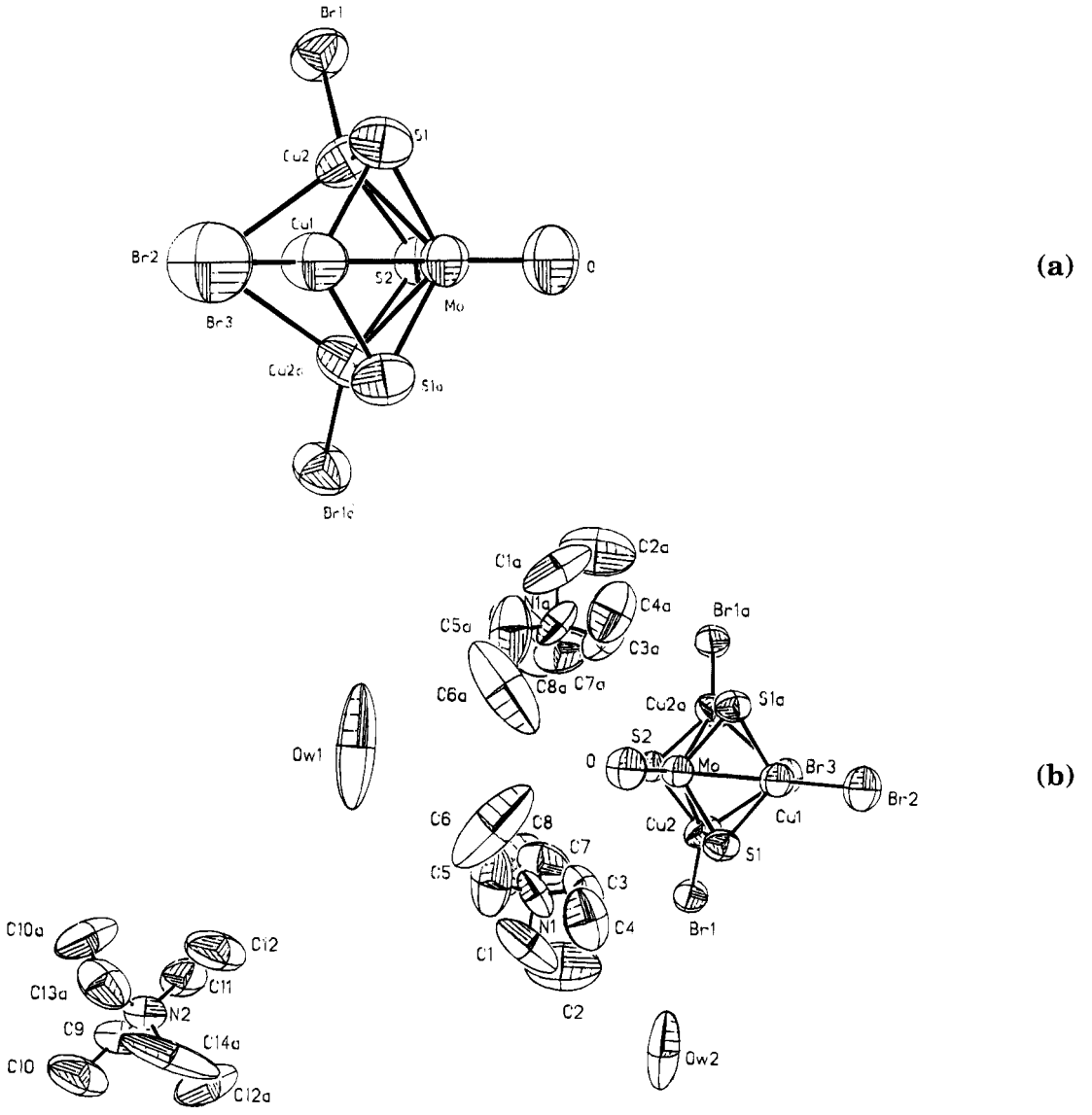

Figure 1. Crystal structures of $[MoOS_3Cu_3Br_3(\mu_2\text{-}Br)]^{3-}$ anion (a), and $(NEt_4)_3[MoOS_3Cu_3Br_3(\mu_2\text{-}Br)]\cdot 2H_2O$ (b).

ral profile of transmitted light pulse should appear much narrower than that of the incident pulse. This is not what we observed. The absence of pulse narrowing of the transmitted laser light rules out thermal lensing process as being responsible for the observed NLO effects. Careful observations also confirm that nonlinear scattering and bubble generation are not important. It is clear that the observed NLO effects of $(NEt_4)_3[MoOS_3Cu_3Br_3(\mu_2\text{-}Br)]\cdot 2H_2O$ are electronic in origin.

Nonlinear Optical Absorption. Typical results of Z-scan experiments are depicted in Figure 4. The nonlinear absorption component was evaluated by a Z-scan method under an open aperture configuration (Figure 4a). The solid line in Figure 4a is a theoretical curve based on eq 5 that describes the third-order NLO absorption of a material.[17,18]

$$T(Z) = \frac{\alpha_0}{\sqrt{\pi}\alpha_2 I_i(Z)(1 - e^{-\alpha_0 L})}\int_{-\infty}^{\infty} \ln\left[1 + \alpha_2 I_i(Z)\frac{(1 - e^{-\alpha_0 L})}{\alpha_0}\right] e^{-\tau^2}\, d\tau \quad (5)$$

where $T(Z)$ is light transmittance, α_0 the linear optical absorptivity, α_2 the effective third-order NLO absorptivity, L the optical path of the sample, and $I_i(Z)$ the on-axis irradiance at position Z. A reasonably good fit between the experimental data (filled circles) and the theoretical curve was obtained, which in turn suggests that the experimentally observed nonlinear absorption is effectively a third-order process. The α_2 value of 1.6 $\times$ 10^{-10} m W^{-1} was derived for the sample from the theoretical curve.

The following two facts strongly suggest that the α_2 value should not correspond to a genuine two-photon absorption coefficient. (1) The cluster exhibits a relatively large linear absorption coefficient at the incident wavelength (see Figure 3). (2) A genuine two-photon absorption generally requires very high incident irradiance.[22,23] Yet in the case of cluster $[MoOS_3Cu_3Br_3(\mu_2\text{-}Br)]^{3-}$, NLO absorption has already become obvious

(22) Ralston, J. M.; Chang, K. R. *Appl. Phys. Lett.* **1969**, *15*, 164.
(23) Van Stryland, E. W.; Wu, Y. Y.; Hagan, D. J.; Soileau, M. J.; Mansour, K. *J. Opt. Soc. Am. B* **1988**, *5*, 1980.

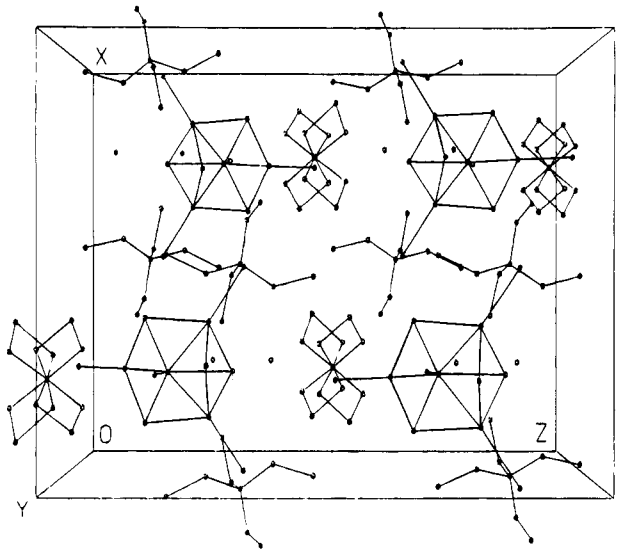

Figure 2. Packing scheme of $(NEt_4)_3[MoOS_3Cu_3Br_3(\mu_2\text{-}Br)]\cdot 2H_2O$ in solid state.

Table 3. Selected Bond Lengths (Å) of $(NEt_4)_3[MoOS_3Cu_3Br_3(\mu_2\text{-}Br)]\cdot 2H_2O$

Mo–Cu(1)	2.645(3)	Mo–Cu(2)	2.663(2)	Mo–S(1)	2.262(4)
Mo–S(2)	2.255(5)	Mo–O	1.693(15)	Mo–Cu(2a)	2.663(2)
Mo–S(1a)	2.262(4)	Br(1)–Cu(2)	2.325(2)	Br(2)–Cu(1)	2.297(4)
Br(3)–Cu(2)	2.870(3)	Cu(1)–S(1)	2.247(4)	Cu(2)–S(1)	2.278(4)
Cu(2)–S(2)	2.276(4)	S(2)–Cu(2a)	2.275(4)		

Table 4. Selected Bond Angles (deg) of $(NEt_4)_3[MoOS_3Cu_3Br_3(\mu_2\text{-}Br)]\cdot 2H_2O$

Cu(1)–Mo–Cu(2)	81.7(1)	Cu(1)–Mo–S(1)	53.8(1)
Cu(2)–Mo–S(1)	54.4(1)	Cu(1)–Mo–S(2)	120.6(2)
Cu(2)–Mo–S(2)	54.4(1)	S(1)–Mo–S(2)	108.2(1)
Cu(1)–Mo–O	129.3(5)	Cu(2)–Mo–O	133.1(3)
S(1)–Mo–O	111.4(3)	S(2)–Mo–O	109.8(5)
Cu(2)–Mo–Cu(2a)	77.8(1)	S(1)–Mo–Cu(2a)	115.5(1)
S(1)–Mo–S(1a)	107.6(2)	Cu(2)–Br(3)–Cu(2a)	71.3(1)
Mo–Cu(1)–Br(2)	167.8(2)	Mo–Cu(1)–S(1)	53.3(1)
Br(2)–Cu(1)–S(1)	124.5(1)	S(1)–Cu(1)–S(1a)	108.7(2)
Mo–Cu(2)–Br(1)	153.9(1)	Mo–Cu(2)–Br(3)	94.5(1)
Br(1)–Cu(2)–Br(3)	111.6(1)	Mo–Cu(2)–S(1)	53.8(1)
Br(1)–Cu(2)–S(1)	120.1(1)	Br(3)–Cu(2)–S(1)	99.7(1)
Mo–Cu(2)–S(2)	53.6(1)	S(1)–Cu(2)–S(2)	107.0(2)
Mo–S(1)–Cu(1)	71.8(1)	Cu(1)–S(1)–Cu(2)	100.2(2)
Mo–S(2)–Cu(2)	72.0(1)	Cu(2)–S(2)–Cu(2a)	94.6(2)

even when the incident irradiance reaches only 40 MW cm^{-2} (see Figure 4). Very likely, the observed NLO absorption is given rise by an excited-state absorption, a process observed in other Mo–Cu–S clusters as well.[9–15] The cluster is stable under room light for weeks but less so toward strong laser pulses. Relatively low incident irradiance and a long time interval (10 s) between pulses were adopted in this study for operational convenience and to ensure an acceptable precision in transmittance measurements.

Nonlinear Optical Refraction. The nonlinear refractive component of $[MoOS_3Cu_3Br_3(\mu_2\text{-}Br)]^{3-}$ was assessed by dividing the normalized Z-scan data obtained under closed-aperture configuration by the normalized Z-scan data obtained under open-aperture configuration (Figure 4b).

The valley and peak occur at equal distances from the focus. This result is consistent with the notion that observed optical nonlinearity has an effective third-order dependence on the incident electromagnetic field.[18] In addition, the valley-peak separation (ΔZ_{v-p}) and the difference of normalized transmittance values at valley and peak positions (ΔT_{v-p}) are found to fit to a set of equations (eqs 6–8) derived for a third-order NLO

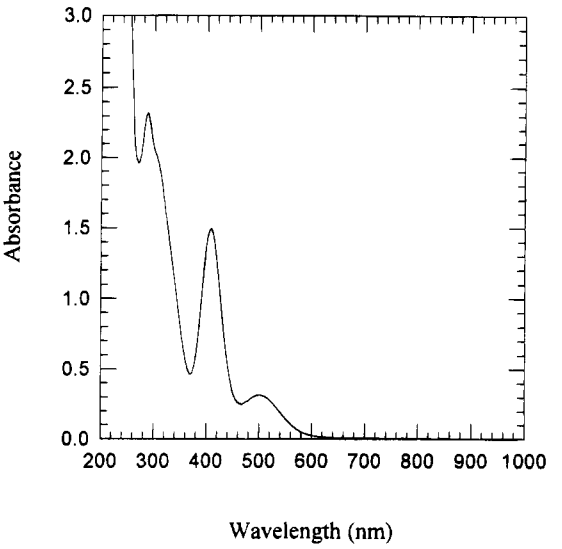

Figure 3. Electronic spectrum of $(NEt_4)_3[MoOS_3Cu_3Br_3(\mu_2\text{-}Br)]\cdot 2H_2O$ (1.9×10^{-3} mol dm^{-3}) in acetonitrile. Optical path is 1 mm.

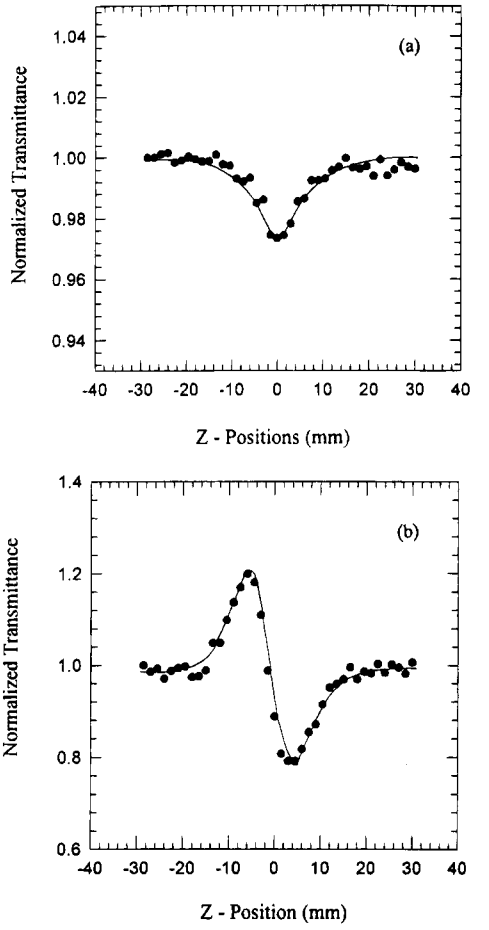

Figure 4. Z-scan data (filled circles) of 1.9×10^{-3} mol dm^{-3} of $(NEt_4)_3[MoOS_3Cu_3Br_3(\mu_2\text{-}Br)]\cdot 2H_2O$, at 532 nm with incident energy of 8 μJ/pulse: (a) collected under open-aperture configuration showing NLO absorption. The solid curve is a theoretical fit based on eq 5; $\alpha_0 = 2.1$ cm^{-1}. (b) Obtained by dividing the normalized Z-scan data obtained under closed-aperture configuration by the normalized Z-scan data in (a). The solid line is an eye guide. The data show self-defocusing effect of the cluster.

$$\Delta Z_{v-p} = 1.72\,\pi\omega_0^2/\lambda \quad (6)$$

$$\Delta T_{v-p} = 0.406|\Delta\Phi_0| \quad (7)$$

$$\Delta\Phi_0 = \frac{2\pi}{\lambda} I_0 \frac{1 - e^{-\alpha_0 L}}{\alpha_0} n_2 \quad (8)$$

process, where λ is the laser wavelength, $\Delta\Phi_0$ and I_0 are the on-axis phase shift and on-axis irradiance, both at focus, respectively.[18]

From eq 8, the effective n_2 value of interest was calculated to be -2.3×10^{-16} m^2 W^{-1}. The negative sign of the effective n_2 value indicates that the cluster can self-defocus laser light propagating through it, a property that has potential for optical limiting applications.

Structure/NLO Correlation. NLO refractive properties observed at wavelengths near a linear optical absorption peak are often influenced by excited-state charge distribution and excited-state lifetime. Composition, symmetry, and rigidity of the cluster structures are important factors in determining the locations and shapes of the potential wells of the excited states, which in turn control the lifetime of the excited states and hence the NLO performance (absorption and refraction) of the clusters in question.

Cubic-cage-shaped clusters have rather rigid structures. Only small structural changes are allowed in these structures when electrons are pumped from ground states to excited states by laser light. Much larger structural deformation is allowed for the nest-shaped clusters. If a large change in charge distribution is to occur upon electronic excitation, a nest-shaped cluster may accommodate this change better than a cubic-cage-shaped cluster and hence allow the excited state to have longer lifetime. Cleavage of one skeletal Cu−Br bond in a cubic-cage cluster resulting in a half-opened cubic cage (structure **V**) whose structural rigidity shall be between that of a cubic-cage cluster and that of a nest cluster (formed from a cubic-cage structure by removal of a skeleton atom and cleavage of three bonds).

Chart 1

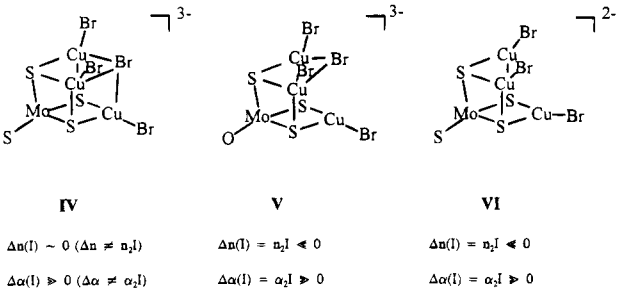

When compared with the NLO properties of cubic-cage and nest-shaped clusters, we noted that $[MoOS_3Cu_3Br_3(\mu_2\text{-}Br)]^{3-}$ resembles the nest-shaped clusters more than the cage-shaped clusters. A general pattern of light dependent refractive index change (Δn) and absorption coefficient change ($\Delta\alpha$) is illustrated in Chart 1.

From the effective α_2 and n_2 values, the effective third-order susceptibility $\chi^{(3)}$ of a 1.9×10^{-3} mol dm^{-3} of $[MoOS_3Cu_3Br_3(\mu_2\text{-}Br)]^{3-}$ was calculated to be 5.4×10^{-10} esu (corresponding effective hyperpolarizability $\gamma = 1.6 \times 10^{-28}$ esu). The $\chi^{(3)}$ values of some best-performing organic polymers and semiconductors are reported at various wavelengths (λ). They are 8.5×10^{-10} for PDA-PTS (at 700 nm), 1.8×10^{-10} for PDA-4BCMU (at 1310 nm), 5.0×10^{-10} for PA (at 1064), and 4.8×10^{-11} for GaAs (at 1064 nm).[24,25]

Supporting Information Available: Tables of crystal cell parameters, bond lengths, bond angles, nonbonding distances, and anisotropic displacement parameters (13 pages); table of observed and calculated structure factors (10 pages). Ordering information is given on any masthead page.

CM950037W

(24) (a) Bredas, J. L.; Adant, C.; Tackx, P.; Persoons, A. *Chem. Rev.* **1994**, *94*, 243. (b) Stegeman, G. L.; Miller, A. In *Physics of All-Optical Switching Devices*; Midwinter, J. E., Ed.; Academic: Orlando, FL, in press.

(25) Adair, R.; Chase, L. L.; Payne, S. A. *Phys. Rev. B* **1989**, *39*, 3337.